RSC Advances

ROYAL SOCIETY OF CHEMISTRY

www.rsc.org/advances

Photoluminescent, self-cleaning titanium oxide nanocomposites for multifunctional properties

Venu Sreekala Smitha, Saju Pillai, Unnikrishnan Nair Saraswathy Hareesh, Balagopal N. Nair and Krishna Gopakumar Warrier*

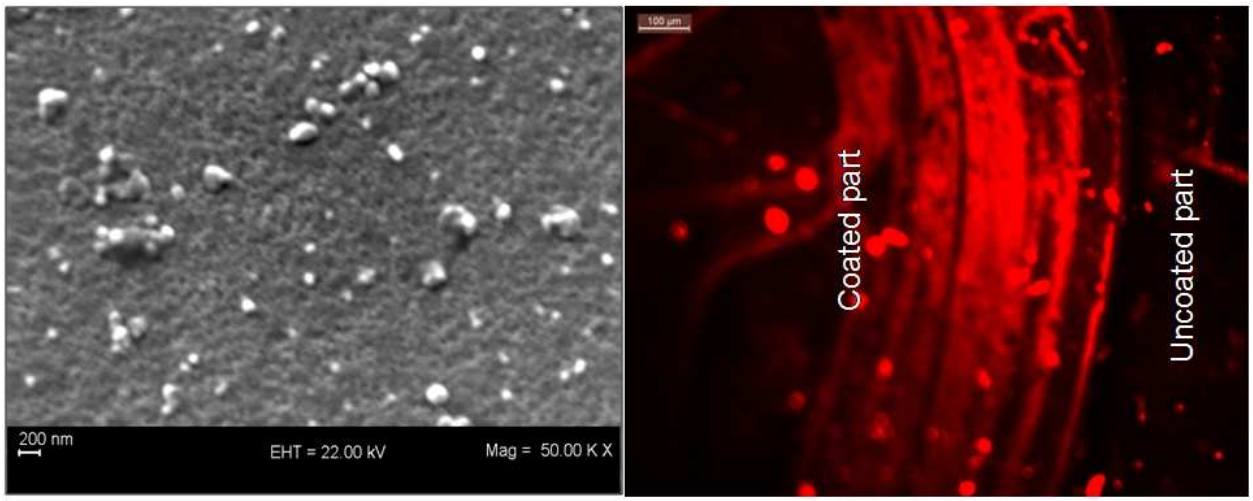

Novel multi functional luminescent and self cleaning composition based on europium doped titania-silica-lanthanum phosphate (TSL) nanocomposite has been synthesized by an aqueous sol-gel process and nanocoatings were fabricated on glass substrates further. Such mesostructured, transparent thin coatings possess photoactivity, low wettability and photoluminescent properties. TSL doped with 1 mol% europium is highly promising for thermally stable, self cleaning luminescent surfaces.

Cite this: DOI: 10.1039/c0xx00000x

www.rsc.org/xxxxxx

ARTICLE TYPE

Photoluminescent, self-cleaning titanium oxide nanocomposites for multifunctional properties

Venu Sreekala Smitha, Saju Pillai, Unnikrishnan Nair Saraswathy Hareesh, Balagopal N. Nair and Krishna Gopakumar Warrier*

Received (in XXX, XXX) Xth XXXXXXXXX 20XX, Accepted Xth XXXXXXXXX 20XX
DOI: 10.1039/b000000x

Photoluminescent and self cleaning properties of Eu^{3+} doped titania-silica-lanthanum phosphate nanocomposite (Eu-TSL) prepared by an aqueous sol-gel process and films fabricated on glass substrates by dip coating are investigated in the present work. These nanocomposites containing Eu^{3+} as dopants exhibit red luminescence upon visible light excitation, after heat treatment at 400 °C. For an excitation wavelength of 465 nm, the PL spectra of Eu-TSL show intense peaks at 613 nm ($^5D_0$-$^7F_2$), characteristic of Eu^{3+} ion. This red emission has a life time of ~0.5 ms. 1 mol% Eu added TSL shows ~96% methylene blue dye degradation under two hours UV light exposure which is attributed to the presence of anatase phase, optimum crystallite size (5.7 nm) and enhanced specific surface area (147 m^2g^{-1}). Eu-TSL was found to be five times efficient in decolourization of methylene blue than Eu-TiO_2 from reported literature. Eu-TSL retains all the major properties including photoactivity, transparency (~97%) and low wettability (~80°). In addition, red emission could be integrated at very low europium doping levels (1 mol%). Even though europium doping on titania is reported widely, a multifunctional luminescent and self cleaning composition based on Eu-TSL synthesized by aqueous sol-gel route is reported for the first time.

1. Introduction

Development of novel multifunctional materials is of considerable interest recently because of the possibility of integration of properties in the form of nanocomposites for different applications.[1-5] Introducing diverse functionality like photoluminescence[6] in photocatalytic titanium dioxide based nanocomposite[7-9] is an apparent way to create novel self-cleaning multifunctional surface. Photoluminescent materials emit light under excitation using an energy source such as photons and are widely used in display devices.[10,11] Lanthanides possess unique orbital arrangement resulting in large stoke's shift and narrow emission, and therefore, has been a natural choice for imparting photoluminescence.[12] Europium ion is a well-known activator for light emitting materials due to their long emission life time and rich spectral properties.[13,14] Eu^{3+} has characteristic luminescence in the red light region.[15-17] The emission from lanthanide ions has been utilized extensively in biological systems.[18] The applications range from luminescent labels of biologically-relevant molecules and the detection of cellular functions.[19] Europium doped inorganic nanoparticles is a new class of fluorescent labelling agent.[20] However, Eu^{3+} does not easily substitute Ti^{4+} due to different chemical properties and ionic radii, and therefore lanthanide ions tend to locate on to the crystal surface leading to formation of nano aggregates of its oxides arising from the interaction between the lanthanide ions. These nano aggregates can further act as luminescent quenching sites.[21,22] Yin et al. demonstrated that mesoporous titania film with semicrystalline framework was an ideal host for lanthanide ions due to the energy transfer from titania nanocrystallite to lanthanide ions in amorphous titania region resulting in an amplified photoluminescence.[23] Thus by integrating the outstanding optical properties of rare-earth ions[24] and photoactive nanoparticles[25] in a nanocomposite, it is possible to develop novel self-cleaning phosphors in the form of coatings or thin films. Such thin films with a high degree of mesoporosity and a broad available surface is pivotal in the fabrication of optical devices which will find wide scope in the areas of sensors,[26] photocatalysis,[27] displays[28] and energy devices.

A nanocomposite of titanium dioxide containing silica and lanthanum phosphate (TSL) is known to exhibit excellent photocatalytic activity and low wetting properties from our previous studies.[3] Hence this composition of titanium oxide has been identified as host for doping europium ions. Titanium dioxide provides photocatalytic property while silica provides better adhesion to the substrate and enables formation of large amount of surface active sites facilitating easy reaction with oxygen and thus leading to enhancement in photocatalytic activity.[9] Lanthanum phosphate is reported to be hydrophobic and in addition, imparts increased anatase phase stability and enhanced hydrophobicity.[25] Hence, in our effort to assimilate additional functionality to titania, effect of addition of europium ions in imparting photoluminescence property to titania

nanocomposite, in addition to the photocatalytic and hydrophobic property of TSL nanocomposite is investigated for the first time in the present work. The nanocomposites showed both self-cleaning property and unique europium fluorescence properties with high emission intensity. Such a multifunctional system can be used in large area display monitors and can have extensive outdoor applications.

2. Experimental Section

2.1. Materials and Methods

The precursor used for the preparation of titanium oxide was titanium (IV) oxysulphate (99.99%, Sigma–Aldrich Chemicals). In a typical experiment, 16 g of titanyl sulphate was dissolved in 500 ml of distilled water to make a 0.2 M solution and was hydrolyzed by slow addition of ammonium hydroxide (25%, s.d. FINE-CHEM Ltd., India) solution under constant stirring at room temperature (32 °C), and was maintained at a stable pH of 7.5. The precipitate obtained was separated by filtration, washed free of sulphate ions with distilled water, as was confirmed by the $BaCl_2$ test. The precipitate was then re-dispersed in 500 ml of distilled water and was peptized by drop wise addition of 2M HNO_3 (Merck, India) solution, till pH is brought down to 1.8 - 2 to get a stable titania sol. The stable sol was then aged for 24 h at room temperature. Ludox^R TM-50 colloidal silica (Aldrich), 50 wt% suspension in water, was used as the silica source. Lanthanum phosphate sol was separately prepared through sol-gel method, by reacting lanthanum nitrate and ortho-phosphoric acid through precipitation-peptization using nitric acid.[29] For the preparation of multifunctional nanocomposite, colloidal silica (44 mol%) and lanthanum phosphate sol (0.5 mol%) were added to the titania sol while keeping the suspension under stirring.[3] Further, definite quantities (0.1, 0.5, 1, 2 and 5 mol%) of europium nitrate solution were added in separate experiments, to the composite TSL sol. This multi-component sol was stirred for two hours and then kept under room temperature (~30 °C) for 24 hours. Part of this was coated on microscopic glass slides by dip coating method in a KSV dip coating unit at a speed of 20 mm per minute providing a retention time of 1 minute. The coated glasses were then dried at 60 °C and further annealed at 400 °C for characterization. The prepared titania-silica-lanthanum phosphate sols were also dried, powdered and calcined at 400 °C and characterized.

2.2. Characterization techniques

Particle size distribution of the nanocomposite sol was measured using photon correlation spectroscopy (Zetasizer 3000 HSA, Malvern Instruments Ltd., UK). X-ray diffraction (XRD) patterns of the calcined composite powders were obtained using a Philips X'pert Pro Diffractometer in the 2θ range 20-60 ° using Cu Kα radiation (λ=1.5406 Å). The crystallite size was calculated using the Scherrer formula given in equation 1:

$$D_{XRD} = 0.9\lambda / \beta \cos\theta \quad (1)$$

where D_{XRD} is the average crystal diameter (nm), 0.9 is the shape factor, λ the X-ray wavelength (Cu Kα, 1.542Å), β is the full width at half maximum intensity (in radian), and θ is the Bragg angle.

The BET (Brunauer, Emmett and Teller) surface area measurements and pore size analysis were carried out by nitrogen adsorption using Micromeritics Gemini 2375 surface area analyzer after degassing each sample at 200 °C for 2 hour. The microstructural details were observed under high resolution transmission electron microscope (HRTEM), FEI Tecnai 30G^{2}S-TWIN operated at an accelerating voltage of 300 kV.

The photocatalytic activity of the nanocomposites was studied by monitoring the degradation of Methylene Blue (MB) (AR Grade, Qualigens Fine Chemicals, India) dye in an aqueous suspension under UV-A and visible light exposure under continuous stirring using a magnetic stirrer. The intensity of the UV light was 0.4 $mWcm^{-2}$. 0.03 g of the prepared nanocomposite was dispersed in 75 ml of 50 μM aqueous solution of MB. The suspension was stirred in the dark for half an hour before irradiating with UV light for equilibration. The concentration of the dye was measured at different time intervals using a UV–Visible spectrometer (Shimadzu, Japan, UV-2401PC). A blank dye solution was also irradiated, for 2 hours to confirm that the dye was not photo bleached by UV exposure. The dye concentration remained unchanged even after irradiation for 2 h. The maximum intensity absorbance peak at 663.2 nm of MB solution was taken for measuring the degradation. The absorbance of MB solution after keeping in dark for half an hour under stirring was taken as initial absorbance (A_0) and absorbance after UV-A exposure in presence of nanocomposites was taken as A (in time intervals of 20 minutes). The degradation of MB was calculated using equation (2):

$$C/C_0 = A_{(time=t)} / A_{(time=0)} \quad (2)$$

where $A_{time=0}$ is the initial absorbance of MB solution, i.e., A_0 and $A_{time=t}$ is the absorbance values after time intervals, i.e., A.

The absorbance and transmittance of the coated samples was recorded by a Shimadzu UV 2401 PC Spectrophotometer (spectral range 200-800 nm). Tauc plot is used to determine the optical band gap. Tauc plot shows the quantity hν (the energy of the light) on the abscissa and the quantity $(\alpha h\nu)^r$ on the ordinate, where α is the absorption coefficient of the material. The value of the exponent r denotes the nature of the transition; for example, r = ½ for indirect transitions. The resulting plot has a distinct linear regime which denotes the onset of absorption. Thus, extrapolating this linear region to the abscissa yields the energy of the optical band gap of the material. SEM images were acquired on an EVO 18 Special Edition scanning electron microscope (Carl Zeiss, Germany) operated at 20kV. The dynamic contact angle measurements of the coated samples were done in Data Physics DCAT $_{21}$ dynamic contact angle meter. The surface roughness of the coatings was measured with atomic force microscopy (AFM). AFM images were obtained using NTEGRA (NT-MDT) instrument. Silicon cantilevers (NSG-10)

with resonance frequency in the range of 190 – 325 kHz and a spring constant in the range of 5.5 – 22.5 Nm^{-1}, and a tip radius of 10 nm were used with a scan rate of 1Hz. AFM imaging was performed in semi-contact mode in air. Fluorescence microscopic images of the samples were recorded in a Spinning Disc Fluorescent Microscope (BD Pathway 855. Bioimager System, USA).

The photocatalytic activity of the nanocomposite coating was studied by monitoring the degradation of standard MB dye. The coated substrate was immersed in MB solution (80 μM) for two minutes and dried, and the initial absorbance of the dye was recorded. The coating stained with dye was then exposed to visible light for two hours in a visible light chamber and the absorbance was taken again. The maximum intensity absorbance peak at 663.2 nm of MB solution was taken for measuring the degradation. The absorbance of MB before irradiation was taken as initial absorbance (A_0) and absorbance after visible light exposure was taken as A. The degradation of MB was calculated then by following equation (2) provided above.

3. Results and Discussion

A constant pH of 1.8 and a constant temperature (30 °C) were maintained while preparing the europium doped TSL compositions. Since the synthesis of europium doped TSL composition contains only sol-solution mixing, the stability of TSL sol after doping with europium ions was ensured by maintaining a pH which is same as that of the undoped sol. Also, the sol was vigorously mixed while the precursor solution is added into the sol for ensuring homogeneity.

3.1. Particle Characterization

Particle size distribution of the TSL nanocomposite sols containing 0.1 and 5 mol% europium ion is presented in Fig. 1 and photographs of the Eu-TSL sols are shown as inset.

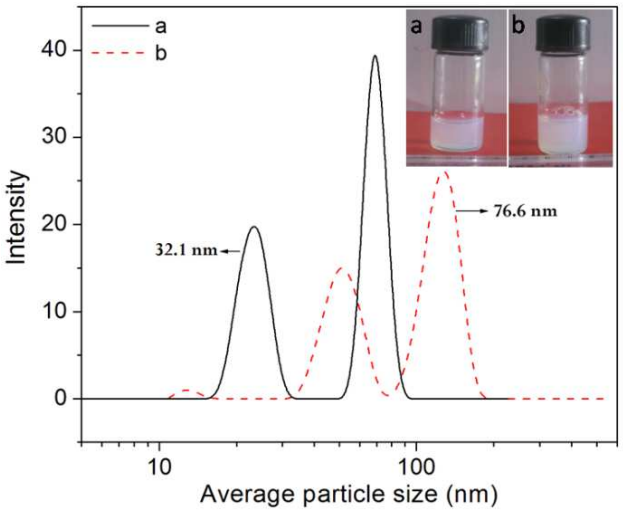

Fig. 1 Particle size analysis of TSL nanocomposite sol containing (a) 0.1 mol% Eu and (b) 5 mol% Eu. Photographs of Eu doped nanocomposite sols containing (a) 0.1 mol% Eu and (b) 5 mol% Eu are shown as inset.

The average particle size of 0.1 mol% Eu containing sol was 32 nm while that containing 5 mol% Eu was 76 nm. The particle size as well as the distribution change with respect to increased europium addition. Sandoval et al. made a similar observation of increased hydrodynamic diameter (305 nm) for a Eu doped core shell titania by dynamic light scattering.[30] The non doped core shell titania had a hydrodynamic diameter (250 nm). This increased hydrodynamic diameter for the Eu-doped hollow nanosphere in the above work was attributed to the accumulation of Eu^{3+} ions on the surface or in the gel coating of the core-shell spheres, with the Eu (III) ions eventually being incorporated into the titania lattice on calcination. Hence the increased average particle size of 5 mol% Eu-TSL sol in the present work could be due to the segregation of Eu (III) ions on the surface of TSL nanocomposites.

X-ray diffraction patterns of the europium doped nanocomposites calcined at 400 °C are provided in Fig. 2. Diffraction peaks of anatase phase at 2θ= 25°as well as traces of brookite were observed in the XRD patterns of pure titania and europium doped TSL nanocomposites. Since calcination of the composite powders has been carried out at 400 °C, phases other than anatase and brookite are not expected here.[3] The crystallinity was further reduced by europium ion doping which is consistent with the report by Leroy et al. where europium ions reduced the crystallization rate of titania.[31]

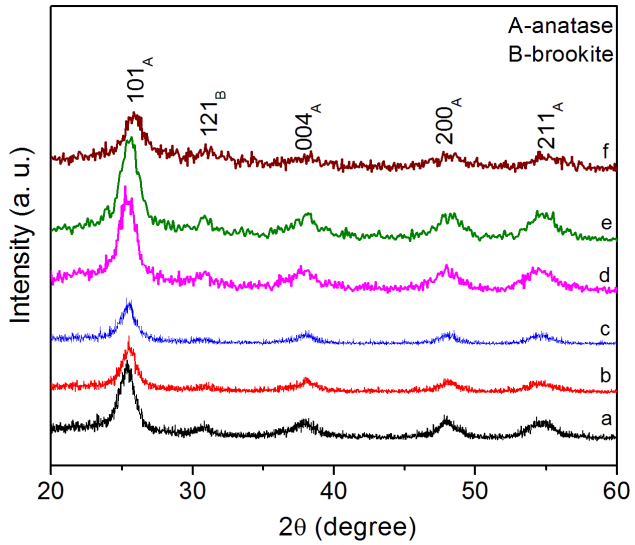

Fig. 2 X-ray diffraction patterns of TSL nanocomposites doped with europium ions (a) 0 mol% (b) 0.1 mol% (c) 0.5mol% (d) 1 mol% (e) 2 mol% and (f) 5 mol%, all calcined at 400 °C.

The solubility of europium in the TiO_2 crystalline phase is low as it does not occupy a crystallographic position in anatase and most likely occupy interstitial sites in anatase, as reported by Ovenstone[32] which reduces the crystallization rate of titania as evident from the decreased crystallinity with respect to europium doping. The anatase crystallite sizes for the undoped and doped composites calcined at 400 °C were calculated further and the results are provided in Fig. 3. For the undoped TSL composite, the anatase crystal size was 5.6 nm.[3] A small amount of europium doping (0.1-0.5 mol%) resulted in an increased crystallite size for

the anatase titania while it decreased for high doping concentration (1-5 mol%). The reduction in crystallite size was only marginal beyond 1 mol% of europium doping. This variation in the anatase crystallite size with respect to Eu doping can be explained in terms of ionic radii of dopant and matrix. Leroy et al. reported that a strong difference in the chemical properties and mismatch in the ionic radii of Eu^{3+} and Ti^{4+} (0.98 and 0.68 Å, respectively) make it difficult to substitute Ti^{4+} by Eu^{3+} within the anatase lattice.[31]

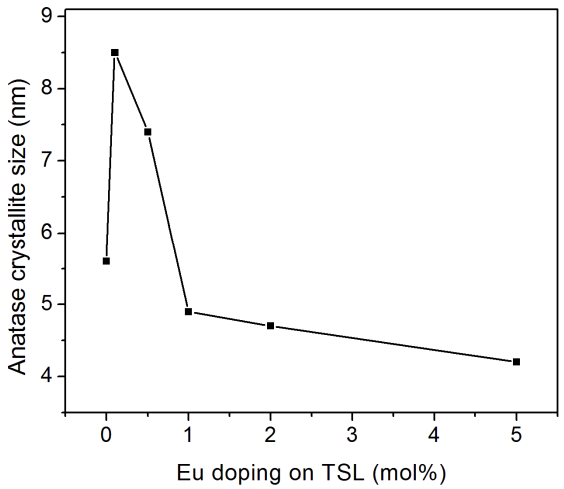

Fig. 3 Variation of anatase crystallite size with respect to Eu doping on TSL composition.

Depending on concentration, Eu^{3+} ions can adopt different environments when incorporated within titania. At very low concentration, the Eu cations will likely enter the titania lattice which is the reason for increased crystal size. Further, it has been reported that when the lanthanide content increases, most of the Eu^{3+} will rather sit close to the semiconductor crystallite surface in a glass like environment,[33] inhibiting the titanium-dioxide crystallization process.[31] The nearly 100% anatase phase observed in the present study can thus be attributed to the presence of Eu^{3+} at the surface of titania crystallites that reduces the anatase crystallite size. Zhang et al. also made similar observation in their studies on europium doped titania in which the particle growth was restrained drastically by europium doping.[34]

TEM analysis of undoped TSL and Eu doped TSL samples were carried out and the results are shown below in Fig. 4-5. Crystallite size reduction by Eu doping on TSL nanocomposite was evident from the TEM images (Fig. 4) and the results were consistent with the XRD results. Anatase crystallite size (D_{TEM}) calculated for undoped TSL was ~11 nm from TEM micrograph which was reduced to ~5 nm for TSL-1Eu nanocomposite. Also, the size of amorphous silica particles (spherical particles with light shade) remains unchanged (~30 nm) with respect to europium addition indicating that the doping of europium ions selectively happens to the crystalline titania matrix thereby changing the anatase crystallite size.

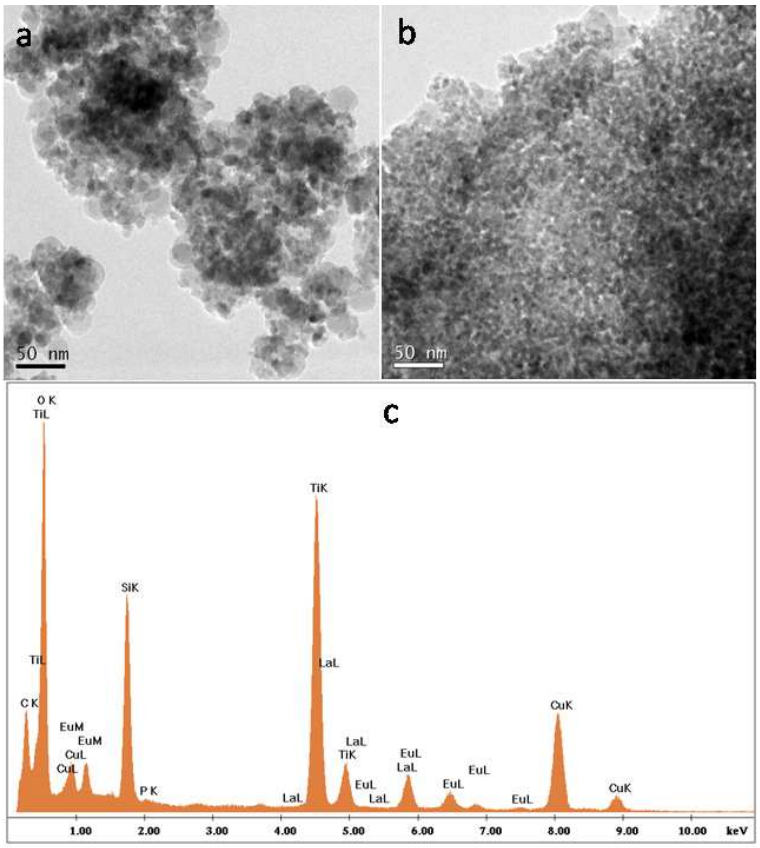

Fig. 4 TEM analysis of (a) undoped TSL and (b) TSL-1Eu, both calcined at 400 °C and (c) EDX spectra of TSL-Eu nanocomposite demonstrating the existence of europium ions.

Cite this: DOI: 10.1039/c0xx00000x

www.rsc.org/xxxxxx

ARTICLE TYPE

EDX analysis (Fig. 4c) also support the existence of TiO_2, SiO_2, $LaPO_4$ and Eu ions in the TSL-Eu nanocomposite. Peaks corresponding to copper and carbon present in the Cu-C grid used for the analysis could also be seen in the spectra. For the undoped TSL nanocomposite (Fig. 5), nanorods of lanthanum phosphate having ~60 nm length and ~10 nm diameter with an interplanar spacing of 0.613 nm, corresponding to the (100) plane of the hexagonal $LaPO_4$ were observed.

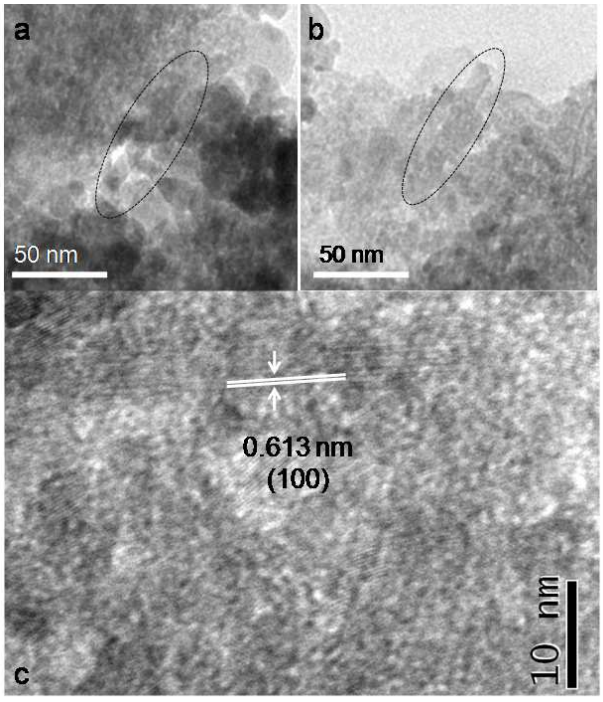

Fig. 5 Magnified TEM images of undoped TSL demonstrating the existence of $LaPO_4$ nanorods (a, b) and (c) lattice fringes corresponding to the (100) plane of hexagonal $LaPO_4$

BET surface area of the pure and europium doped TSL nanocomposites are presented in Table 1.

Table 1 Textural characteristics of europium doped TSL nanocomposites calcined at 400 °C.

Sample ID	BET surface area (m^2g^{-1})	Total pore volume (cm^3g^{-1})	Micro pore volume (cm^3g^{-1})	Meso pore volume (cm^3g^{-1})	Pore diameter (nm)
TSL-0Eu	138.5	0.24809	-0.00087	0.24896	6.3
TSL-0.1Eu	122.9	0.16891	-0.00217	0.17109	4.8
TSL-0.5Eu	134.1	0.17497	-0.00325	0.17823	4.5
TSL-1Eu	147.3	0.16265	-0.00424	0.16689	3.7
TSL-2Eu	135.9	0.15767	-0.00354	0.16121	3.9
TSL-5Eu	121.5	0.15470	-0.00295	0.15765	4.5

The doped as well as undoped TSL nanocomposites were mesoporous in nature as revealed from the hysteresis loop (Type IV adsorption-desorption isotherm). BET surface area was maximum for the TSL composite doped with 1 mol% Eu and the average pore diameter was also less (3.7 nm) when compared with other samples with lower and higher europium loading. The high surface area of 1 mol% europium doped sample is due to the decreased particle size, which is consistent with the results of XRD and TEM. This mesoporous structure of the europium doped TSL nanocomposites is highly beneficial for the photocatalytic activity.[35]

The photocatalytic activity of undoped and europium doped TSL nanocomposites were also evaluated by monitoring the degradation of an aqueous solution of a standard dye methylene blue. The degradation of dye solution upon UV-A irradiation (2 hours) by the samples are presented in Fig. 6.

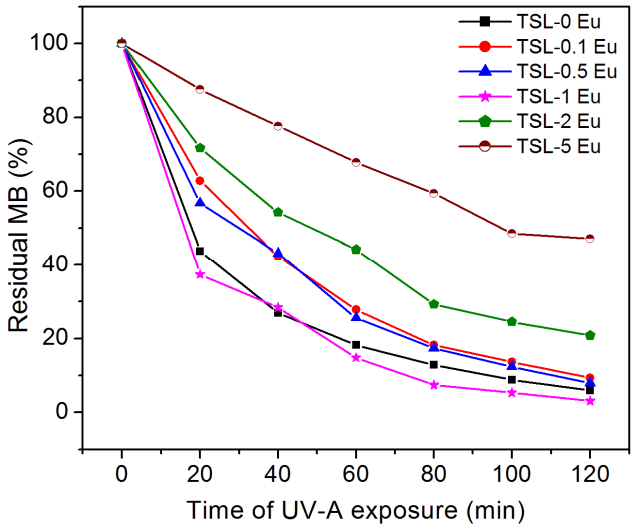

Fig. 6 Methylene blue degradation of undoped and Eu doped TSL nanocomposites, all calcined at 400 °C and subjected to UV-A exposure.

0.1 to 0.5 mol% doping of Eu^{3+} ions resulted in comparable photoactivity with that of undoped TSL. A higher photocatalytic activity than that of undoped TSL was exhibited by TSL-1Eu and this enhanced photocatalytic activity can be attributed to the presence of nearly 100% anatase, optimum crystallite size and increased surface area[36] achieved by the europium doping. The enhanced surface area of 147 m^2g^{-1} in the case of TSL-1Eu may increase the photocatalytic activity since the number of active sites on which the electron acceptor and donor are adsorbed and participate in the redox reaction will be increased.[37] The effectiveness of Eu doped TSL in decolourization of methylene blue was higher than those reported for Eu doped mesoporous titanium dioxide prepared by sol-gel method.[18] Table 2 shows a comparison between Eu doped mesoporous titania from a reported literature and Eu doped TSL in the present work. Enhanced methylene blue degradation efficiency was observed for the TSL-1Eu sample, when compared with Eu-TiO_2[18] under

similar light source and irradiation time, but with a very low catalyst loading of 0.02 g/ 50 ml. In both the cases, a nearly similar dye concentration was used and TSL-1Eu can be considered as five times efficient over Eu-TiO_2 with reference to its very low catalyst loading.

Table 2 Comparison of photocatalytic activity of TSL-1Eu in the present work with Eu-TiO_2 from reported work.

Sample	Catalyst dosage	Dye concentration	Light source and time of irradiation	MB degradation
Eu –TiO_2	0.1g / 50 ml	20 mg / L	UV-A, 2h	95%
TSL-1Eu	0.02 g / 50 ml	16 mg / L	UV-A, 2h	97%

However, the photocatalytic activity was not proportional to the europium concentration. Apart from the concentration of europium ions, the manner in which Eu^{3+} exists also may play important role in the photocatalytic activity of europium doped TSL.[31] However, europium ions forming the Ti–O–Eu bond should be greatly changed with respect to the concentration of europium and should exert appreciable influence on the activity of the TSL nanocomposite. Substitution of Ti^{4+} by Eu^{3+} may get saturated at a certain level of europium loading considering the large mismatch in the ionic radii of Ti^{4+} and Eu^{3+} which will probably induce a maximum value for the photocatalysis.[34]

The photoluminescence spectra of the europium doped TSL nanocomposites calcined at 400 °C is provided in Fig. 7 and the corresponding excitation spectra are given as inset. For obtaining the emission spectra, an excitation at 465 nm was followed since the excitation spectra show maximum intensity peak at 465 nm (inset of Fig. 7).

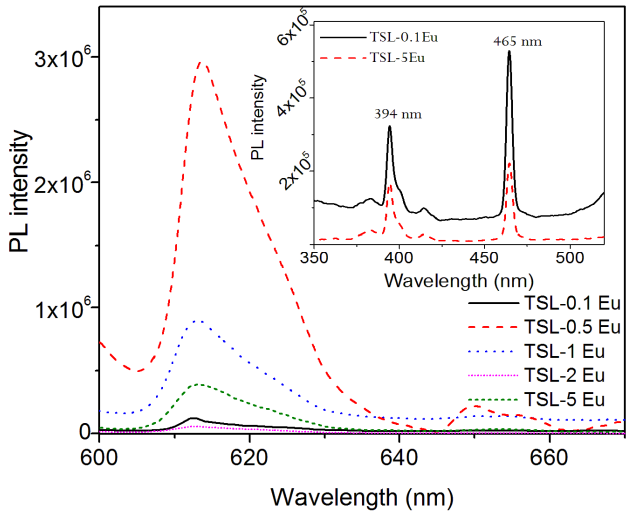

Fig. 7 Room temperature PL spectra of the europium doped TSL nanocomposites calcined at 400 °C (Excitation spectra of the Eu doped TSL nanocomposites are shown as inset).

Eu^{3+} doped TSL nanocomposite shows sharp and well resolved emission peaks corresponding to the radiative relaxations from the $^5D_0$ level of the Eu^{3+} ions to its low lying multiplets ^7F_j. The strongest emission centered at around 613 nm is due to the electrical dipole transition ($^5D_0$ - $^7F_2$) of Eu^{3+} ions that gives a red emission.[16] The other emission peak centered at 651 nm is associated with the ($^5D_0$ - $^7F_3$) transition of Eu^{3+} ions.

TSL-1Eu composite powder was further observed under fluorescence microscope and the life time measurement of fluorescence was also carried out. The results are presented in Fig. 8.

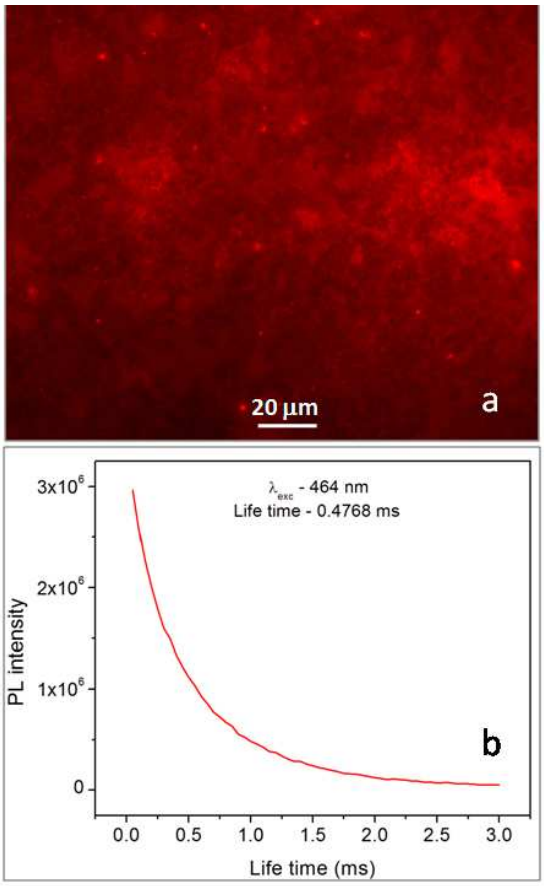

Fig. 8 Characterization of 1 mol% europium doped TSL nanocomposite calcined at 400 °C (a) Fluorescence microscopic image (b) life time decay curve.

Intense red emission was observed when the powder sample was excited at 484 nm and the obtained result was in agreement with the powder PL data. Also, the europium doped nanocomposite containing 1 mol% europium has a life time of ~0.5 ms. Sandoval et al. also reported an intense red emission for Eu doped titania nano shells when observed under a fluorescence microscope.[30]

3.2. Characterization of Eu-TSL coating

SEM and fluorescence microscopic analyses of TSL-1Eu composite coating annealed at 400 °C were carried out and the results are presented in Fig. 9. The europium doped composite coating was highly porous with pore size less than 50 nm. This mesoporous behaviour of the coating can be justified by the BET surface area results that revealed the presence of large amount of mesopores. The fluorescence microscopic image of TSL-1Eu composite coating also shows intense red emission when excited at 484 nm. The emission characteristic of the nanocomposite coating is clearly understood from Fig. 9b.

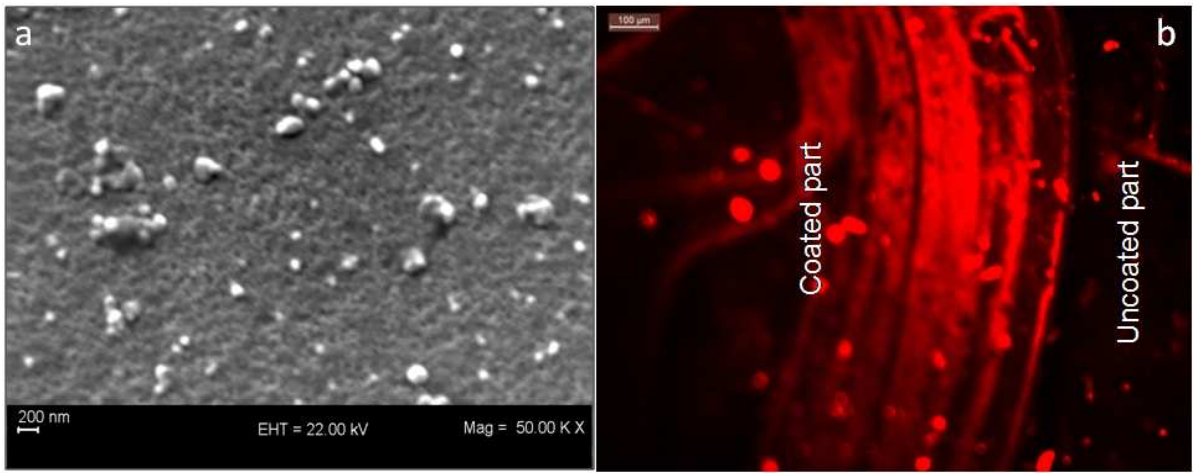

Fig. 9 Characterization of TSL-1Eu composite coating annealed at 400 °C (a) SEM image and (b) Fluorescent microscopic image.

The AFM surface images of the TSL-1Eu nanocomposite coating shows the presence of uniformly arranged particles (Fig. 10). Some larger agglomerates revealing the existence of europium oxide on the surface or in the pores of titania crystallites as reported by Leroy et al.[31] were observed in the present case also.

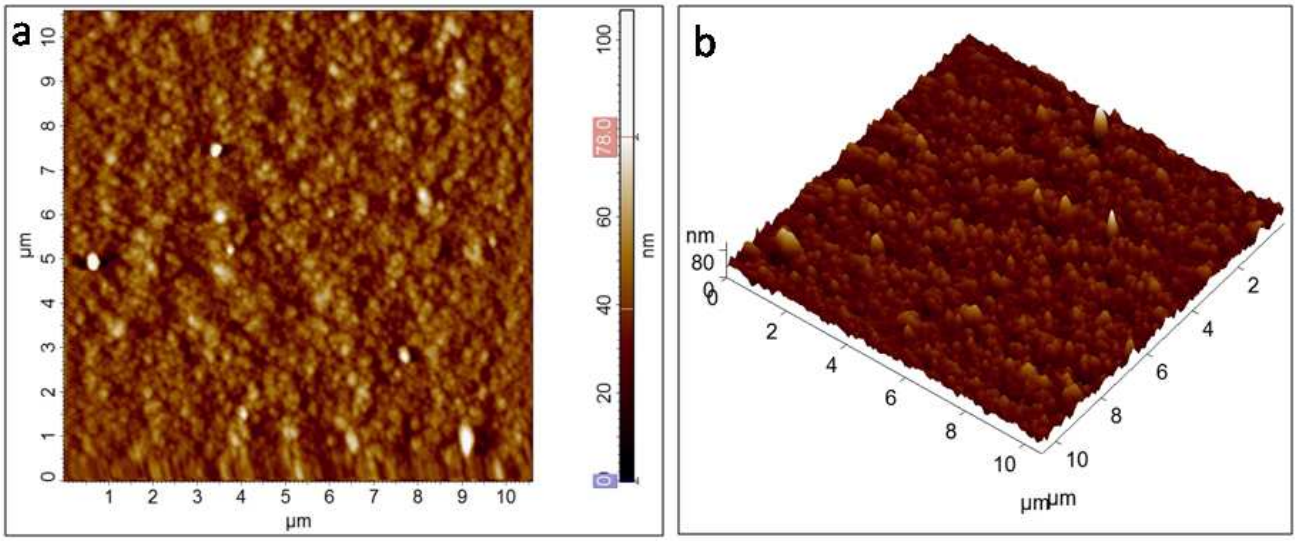

Fig. 10 AFM analysis of TSL-1Eu composite coating, annealed at 400 °C (a) surface image and (b) three dimensional image.

The UV-visible transmittance and the tauc plot of the TSL-1Eu composite coating are provided below in Fig. 11. A relative transparency reduction of ~3% was observed for TSL-1Eu composite coating which is attributed to the presence of agglomerated particles on the surface of titania as can be seen from SEM and AFM.

The band gap energy calculated from the tauc plot is 3.4 eV for the TSL-1Eu composite as against 3.6 eV for the undoped TSL composite. This red shift in the band gap energy value indicated an absorbance towards visible region.[38]A relative transparency reduction of ~3% was observed for TSL-1Eu composite coating which is attributed to the presence of agglomerated particles on the surface of titania as can be seen from SEM and AFM. The band gap energy calculated from the tauc plot is 3.4 eV for the TSL-1Eu composite as against 3.6 eV for the undoped TSL composite. This red shift in the band gap energy value indicated an absorbance towards visible region.[38]

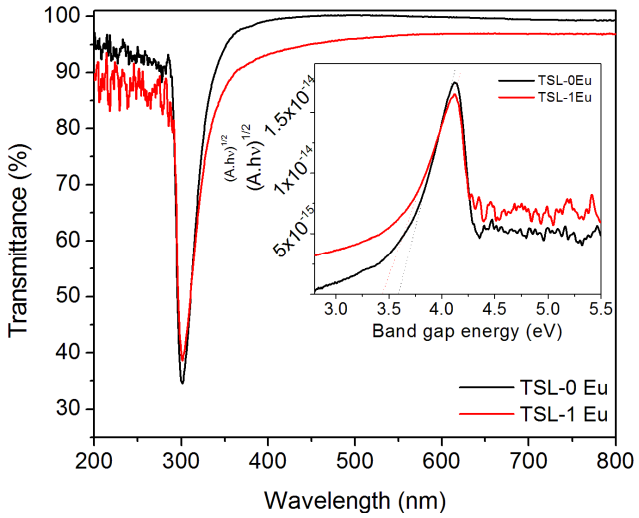

Fig. 11 UV-Visible transmittance of undoped TSL and TSL-1Eu composite coating on glass, annealed at 400 °C. (Tauc plot of undoped and TSL-1Eu composite coating is provided as inset).

The photocatalytic activity of the TSL-1Eu coating evaluated by methylene blue degradation under visible light shows degradation efficiency of ~46% over an exposure time of two hours (Fig. 12). Chi et al. demonstrated that nitrogen and europium doped titania anodized films has got a dye (aniline blue) degradation efficiency of ~45% (dye concentration – 85 μM) under visible light exposure for two hours.[39] In the present study, we could achieve nearly same dye (methylene blue) degradation efficiency (dye concentration 80 μM) for the TSL-1Eu composite coating, under two hours visible light exposure, even without addition of any non-metal dopants that significantly changes the band gap of titania towards visible region. One of the reasons for the lower dye degradation efficiency of composite coating compared with that of powder sample (~96%) is due to the very low amount of titania present in the nanocoating.[9] The water contact angle measured for TSL-1Eu composite coating was 80 ° compared to ~83 ° for the undoped TSL coating[3] which shows that europium doping of TSL nanocomposite still retains all the major properties of TSL composite coating. In addition, red emission could be integrated at very low Eu doping levels (1 mol%).

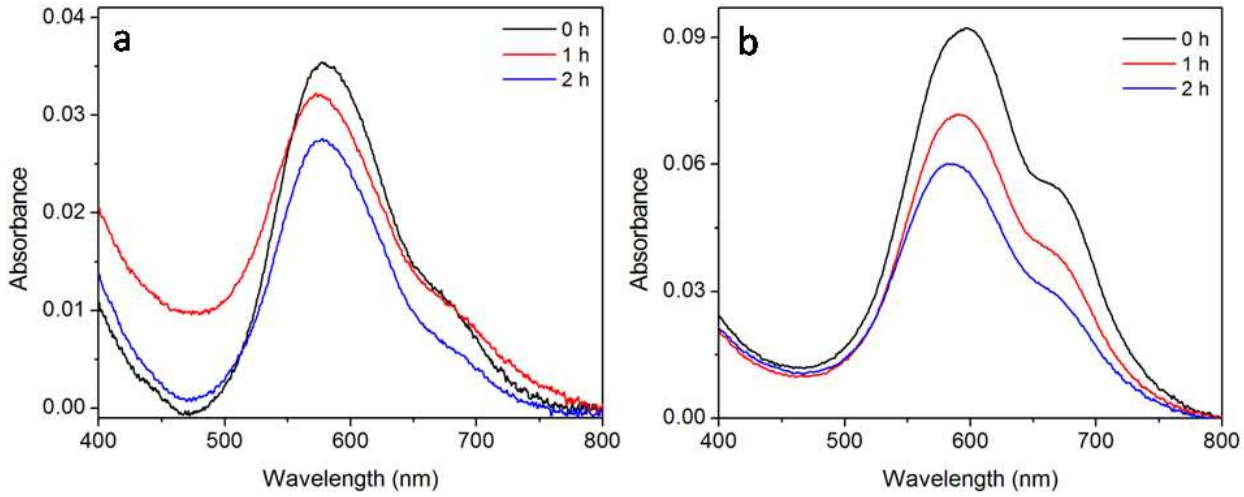

Fig. 12 Methylene blue degradation by (a) pure titania and (b) TSL-1Eu nanocomposite coating under 2h visible light exposure.

Such meso-structured transparent thin coatings possessing photocatalytic activity and low wettability along with photoluminescent properties can be effectively used in many multifunctional applications.

Conclusions

A multi functional luminescent and self cleaning composition based on europium doped TSL nanocomposite was successfully synthesized by an aqueous sol-gel process. Further, sol–gel-derived films were fabricated onto glass substrates by dip coating method and such coatings also possessed multifunctional properties. Red emission was observed on visible light excitation of the europium doped TSL heated to 400 °C. For an excitation wavelength of 465 nm, the PL spectra of Eu-TSL show intense peaks at 613 nm ($^5D_0$-$^7F_2$), characteristic of trivalent europium ions. Europium doping of the TSL nanocomposite resulted in a small red shift in the band gap energy indicating visible light activity. Moreover, the rare earth doped TSL composites exhibited mesoporous structure as revealed from SEM, BET surface area and pore size distribution analyses. Such mesostructured, transparent (~97%) thin coatings possessing photocatalytic activity (~96%) and low wettability (~80 °) along with photoluminescent properties (red emission) can satisfy multifunctional applications. Hence TSL nanocomposite doped with low amount of europium is a promising material for further development to self cleaning and luminescent applications, even at higher temperatures compared to some of the organic hybrid coatings.

Acknowledgments

Authors V. S. Smitha and K. G. K. Warrier acknowledge HRDG, CSIR, India, for providing financial support in the form of Senior Research Fellowship and Emeritus's Scientist Project respectively. The authors further acknowledge the members of

Materials Science and Technology Division, NIIST-CSIR for providing general assistance. Mrs. Lucy Paul, Mr. Kiran, Ms. Vineetha and Mr. Deepak are being acknowledged for extending the instrumental facilities for SEM, TEM, Fluorescence microscopy and PL measurements respectively.

Notes and references

[a] *Materials Science and Technology Division, National Institute for Interdisciplinary Science and Technology, (CSIR), Thiruvananthapuram - 695 019, India. Fax: +91-471-2491712; Tel: +91-471-2515280; E-mail: warrier@niist.res.in*

1 M. Faustini, L. Nicole, C. Boissiere, P. Innocenzi, C. Sanchez and D. Grosso, *Chem. Mater.,* 2010, **22**, 4406.
2 D. Lee, M. F. Rubner and R. E. Cohen, *Nano Lett.* 2006, **6**, 2305.
3 V. S. Smitha, C. K. Jyothi, P. Mohamed A, S. Pillai and K. G. Warrier, *Dalton Trans.,* 2013, **42**, 4602.
4 V. S. Smitha, K. V. Baiju, P. Perumal, S. Ghosh and K. G. Warrier, *Eur. J. Inorg. Chem.,* 2012, **2012**, 226.
5 M. E. A. Warwick, C. W. Dunnill and R. Binions, *Chem. Vap. Deposition,* 2010, **16**, 220.
6 K. L. Frindell, M. H. Bartl, A. Popitsch and G. D. Stucky, *Angew. Chem., Int. Ed.,* 2002, **41**, 959.
7 V. S. Smitha, K. B. Jaimy, P. Shajesh, J. K. Jeena and K. G. Warrier, *J. Mater. Chem. A,* 2013, **1**, 12641.
8 V. S. Smitha, P. Francois, U. N. S. Hareesh and K. G. Warrier, *J. Mater. Chem. A,* 2013, **1**, 12178.
9 V. S. Smitha, K. A. Manjumol, K. V. Baiju, S. Ghosh, P. Perumal and K. G. K. Warrier, *J. Sol-Gel Sci. Technol.,* 2010, **54**, 203.
10 H. J. Queisser, *J. Lumin.,* 1981, **24-25, Part 1**, 3.
11 C. Feldmann, T. Jüstel, C. R. Ronda and P. J. Schmidt, *Adv. Funct. Mater.,* 2003, **13**, 511.
12 J. C. G. Bunzli and C. Piguet, *Chem. Soc. Rev.,* 2005, **34**, 1048.
13 M. Pal, U. Pal, J. M. Gracia Y Jimenez and F. Perez-Rodriguez, *Nanoscale Res. Lett.,* 2012, **7**, 1.
14 I. Cacciotti, A. Bianco, G. Pezzotti and G. Gusmano, *Mater. Chem. Phys.,* 2011, **126**, 532.
15 D. Chen, Q. Zhu, Z. Lv, X. Deng, F. Zhou and Y. Deng, *Mater. Res. Bull.,* 2012, **47**, 3129.
16 C. Leostean, M. Stefan, O. Pana, A. I. Cadis, R. C. Suciu, T. D. Silipas and E. Gautron, *J. Alloys Compd.,* 2013, **575**, 29.
17 Y. Wang, Y. Guo, G. Wang and F. Wang, *J. Nanosci. Nanotechnol.,* 2011, **11**, 3162.
18. F. Wang, W. B. Tan, Y. Zhang, X. Fan and M. Wang, *Nanotechnol.,* 2006, **17**, R1.
19. Z. Y. Ma, D. Dosev, M. Nichkova, S. J. Gee, B. D. Hammock and I. M. Kennedy, *J. Mater. Chem.*, 2009, **19**, 4695.
20. J. Yang, S. Sandoval, J. G. Alfaro, S. Aschemeyer, A. Liberman, D. T. Martin, M. Makale, A. C. Kummel and W. C. Trogler, *J Biomed Opt.*, 2011 **16**, 066012.
21 J. Ovenstone, P. J. Titler, R. Withnall and J. Silver, *J. Mater. Res.,* 2002, **17**, 2524.
22 H. Zhao, C. Jia, H. Duan, Z. Sun, X. Wang and E. Xie, *J. Alloys Compd.,* 2008, **455**, 497.
23 J. Yin, L. Xiang and X. Zhao, *Appl. Phys. Lett.,* 2007, **90**, 113112.
24 A. Lauria, I. Villa, M. Fasoli, M. Niederberger and A. Vedda, *ACS Nano,* 2013, **7**, 7041.
25 C. K. Jyothi, K. B. Jaimy, S. Ghosh, S. Sankar, V. S. Smitha and K. G. K. Warrier, *J. Solid State Chem.,* 2011, **184**, 1867.
26 J. Yu, L. Sun, H. Peng and M. I. J. Stich, *J. Mater. Chem.,* 2010, **20**, 6975.
27 A. Podhorodecki, G. Zatryb, P. Sitarek, J. Misiewicz, D. Kaczmarek, J. Domaradzki, A. Borkowska and E. L. Prociow, *Thin Solid Films,* 2009, **517**, 6331.
28 J. L. Ferrari, M. A. Schiavon, R. R. Goncalves, A. M. Pires and M. R. Davolos, *Thin Solid Films,* 2012, **524**, 299.
29 K. Rajesh, P. Shajesh, O. Seidel, P. Mukundan and K. G. K. Warrier, *Adv. Funct. Mater.,* 2007, **17**, 1682.
30 S. Sandoval, J. Yang, J. G. Alfaro, A. Liberman, M. Makale, C. E. Chiang, I. K. Schuller, A. C. Kummel and W. C. Trogler, *Chem. Mater.,* 2012, **24**, 4222.
31 C. M. Leroy, T. Cardinal, V. Jubera, M. Treguer-Delapierre, J. Majimel, J. P. Manaud, R. Backov, C. Boissiere, D. Grosso, C. Sanchez, B. Viana and F. Pelle, *ChemPhysChem,* 2008, **9**, 2077.
32 J. Ovenstone, P. J. Titler, R. Withnall and J. Silver, *J. Phys. Chem. B,* 2001, **105**, 7170.
33 K. L. Frindell, M. H. Bartl, M. R. Robinson, G. C. Bazan, A. Popitsch and G. D. Stucky, *J. Solid State Chem.,* 2003, **172**, 81.
34 Y. H. Zhang, H. X. Zhang, Y. X. Xu and Y. G. Wang, *J. Mater. Chem.,* 2003, **13**, 2261.
35 K. Liu, L. Zhu, T. Jiang, Y. Sun, H. Li and D. Wang, *Int. J. Photoenergy,* 2012, **2012**, 1.
36 P. Periyat, K. V. Baiju, P. Mukundan, P. K. Pillai and K. G. K. Warrier, *Appl. Catal., A,* 2008, **349**, 13.
37 L. Q. Mao, Q. L. Li, H. X. Dang and Z. J. Zhang, *Mater. Res. Bull.,* 2005, **40**, 201.
38 H. Shi, T. Zhang and H. Wang, *J. Rare Earth.,* 2011, **29**, 746.
39 C. S. Chi, J. Choi, Y. Jeong, O. Y. Lee and H. J. Oh, *Thin Solid Films,* 2011, **519**, 4676.